EUROPEAN COOPERATION
IN THE FIELD OF SCIENTIFIC
AND TECHNICAL RESEARCH

COST 2100 TD(07)336
Duisburg, Germany
Sep 10-11, 2007

EURO-COST

SOURCE: Forschungszentrum Telekommunikation Wien (ftw.), Vienna, Austria

Institut für Nachrichtentechnik und Hochfrequenztechnik, Technische Universität Wien, Vienna, Austria

Department of Electrical and Information Technology, Lund University, Lund, Sweden

FOI Swedish Defence Research Agency, Linköping, Sweden

Elektrobit, Finland

Tracking Time-Variant Cluster Parameters in MIMO Channel Measurements: Algorithm and Results

Nicolai Czink, *et al.*
Donau-City-Straße 1, 1220 Wien, Austria
Phone: +43 (1) 5052830 19
Fax: +43 (1) 5052830 99
Email: czink@ftw.at

Tracking Time-Variant Cluster Parameters in MIMO Channel Measurements: Algorithm and Results

Nicolai Czink[1,2], Ruiyuan Tian[3], Shurjeel Wyne[3], Gunnar Eriksson[3,4], Fredrik Tufvesson[3], Thomas Zemen[1], Jukka-Pekka Nuutinen[5], Juha Ylitalo[5], Ernst Bonek[2], Andreas F. Molisch[3]

[1]Forschungszentrum Telekommunikation Wien (ftw.), Vienna, Austria
[2]Institut für Nachrichtentechnik und Hochfrequenztechnik, Technische Universität Wien, Vienna, Austria
[3]Department of Electrical and Information Technology, Lund University, Lund, Sweden
[4]FOI Swedish Defence Research Agency, Linköping, Sweden
[5]Elektrobit, Finland

Abstract

This paper presents a joint clustering-and-tracking framework to identify time-variant cluster parameters for geometry-based stochastic MIMO channel models.

The method uses a Kalman filter for tracking and predicting cluster positions, a novel consistent initial guess procedure that accounts for predicted cluster centroids, and the well-known KPower-Means algorithm for cluster identification.

We tested the framework by applying it to three entirely different sets of MIMO channel measurement data obtained by different channel sounders: indoor measurements conducted at 2.55 GHz, outdoor rural measurements at 300 MHz, and outdoor sub-urban measurements at 2.0 GHz. The time-variant cluster parameters of interest are: (i) cluster movement, (ii) change of cluster spreads, (iii) cluster lifetimes, and birth and death rates of cluster.

We find that clusters show significant movement in parameter space depending on the environment. The spreads of individual clusters change rather randomly over their lifetime, with a standard deviation up to 150% of their mean spread. The cluster lifetime is approximately exponentially distributed, however additionally one has to account for long-living clusters coming from the line-of-sight path or from major reflectors.

1 Introduction

In order to validate algorithms that exploit the opportunities offered by MIMO systems, MIMO channel models that are accurate, yet tractable are in high need. A promising approach involves cluster-based MIMO channel models [1]. As a matter of fact, the majority of standardized MIMO channel models, like 3GPP-SCM [2], IEEE 802.11n [3], COST 259 DCM, and COST 273 [4] are cluster based.

In measured MIMO channels the multipath components (MPCs) tend to occur in clusters, i.e., groups of MPCs with similar parameter values such as delay, directions of arrival (DoA) and

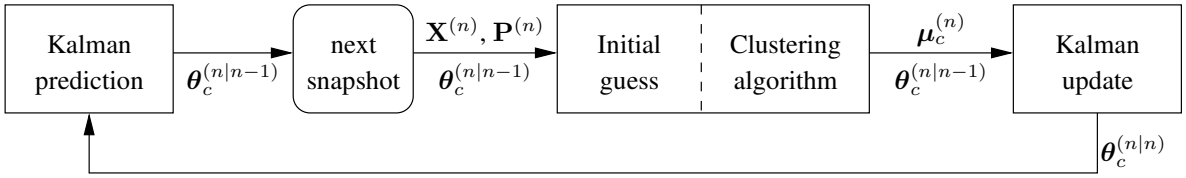

Figure 1: Clustering framework: Clusters with parameters $\boldsymbol{\theta}_c^{(n)}$ are identified and tracked in the input data $(\mathbf{X}^{(n)}, \mathbf{P}^{(n)})$, the Kalman filter updates the cluster parameters, the prediction provides an input to the initial guess.

directions of departure (DoD) [5, 6, 7]. It was shown in [8, 9] that channel models disregarding clustering effects overestimate the channel capacity.

In order to consistently parametrize recent cluster-based MIMO channel models [10], the clusters must be identified and parametrized from measurements. Initially, cluster identification was done visually [11, 6, 7], but this procedure is cumbersome and tiring for a large amount of measurement data, and for multi-dimensional parametric data it becomes practically impossible. Moreover, visual clustering lacks a clear definition of what a cluster is. Thus, automatic cluster identification algorithms for parametric MIMO channels were developed [12, 13, 14]. These algorithms were all designed to identify clusters in individual time instants, and did not address the issue of cluster tracking over time. Since clusters can be used to model time-variant scenarios as well, a consistent approach is required for joint cluster identification-and-tracking over time. A simple cluster tracking algorithm was presented in [15], but it did not take joint clustering and tracking into account. An alternative method is to track individual paths directly in the impulse response [16].

In the present work we develop a joint clustering-and-tracking framework that uses (i) a Kalman filter [17] to track and predict cluster positions together with (ii) a new initial-guess procedure allowing to include the prediction of the Kalman filter, and (iii) the KPowerMeans clustering algorithm using the MCD distance metric [13] to identify clusters. To test the framework we used three different sets of time-variant MIMO channel measurements, one indoor environment measured at 2.55 GHz showing rich scattering, an outdoor environment measured at 2.0 GHz showing few, very distinct propagation paths and many weak scattered paths, and another outdoor rural environment measured at 300 MHz. We found that this framework enabled to extract the cluster characteristics from time-variant MIMO channel measurements consistently.

The paper is organized as follows: Section 2 will describe the problem and introduce the parameters used. In Section 3 we provide a comprehensive description of the joint clustering-and-tracking framework. An overview of the three different MIMO channel measurements is provided in Section 4. Results from applying the framework to the measurement data are presented in Section 5. Finally, we conclude the paper in Section 6.

2 Problem description

Like in existing clustering applications, the starting point is a large number of measurements with a MIMO channel sounder. The parameters of the MPCs are estimated from the measured impulse responses using a high-resolution algorithm, e.g. SAGE, for each snapshot, individually.

In standard clustering, each snapshot is clustered independently [18, 13], and the clusters might be tracked afterwards [14]. The problem to solve is how to combine clustering and tracking in order to improve the clustering performance and to consistently track clusters.

We consider N data windows, $n = 1 \dots N$, each with a number of $L^{(n)}$ MPCs, where every single MPC is represented by its power $P_l^{(n)}$, $l = 1 \dots L^{(n)}$, and a parameter vector $\mathbf{x}_l^{(n)} = [\tau_l^{(n)} \ \varphi_{\mathrm{Rx},l}^{(n)} \ \varphi_{\mathrm{Tx},l}^{(n)}]^{\mathrm{T}}$ containing the delay, azimuth AoA and azimuth AoD, respectively. The data for all paths are collected in the power vector $\mathbf{P}^{(n)} = [P_1^{(n)} \dots P_L^{(n)}]^T$ and the matrix $\mathbf{X}^{(n)} = [\mathbf{x}_1^{(n)} \dots \mathbf{x}_L^{(n)}]^T$.

Each *cluster* is determined by following parameters:

1. A *unique cluster-ID* c.

2. The *cluster power* at time n. Denoting the set of path indices belonging to cluster c at time snapshot n by $\mathcal{I}_c^{(n)}$, the cluster power is calculated as $\gamma_c^{(n)} = \sum_{l \in \mathcal{I}_c^{(n)}} P_l^{(n)}$.

3. The *number of paths* within the clusters $L_c^{(n)} = |\mathcal{I}_c^{(n)}|$, where every path is assumed to belong to one cluster, uniquely.

4. The *cluster centroid* position in the angle-angle-delay domain $\boldsymbol{\mu}_c^{(n)}$. The cluster centroid position can be calculated as

$$\begin{aligned} \boldsymbol{\mu}_c^{(n)} &= [\tau_c^{(n)} \ \varphi_{\mathrm{Rx},c}^{(n)} \ \varphi_{\mathrm{Tx},c}^{(n)}]^{\mathrm{T}} = \\ &= \begin{bmatrix} \frac{1}{\gamma_c^{(n)}} \cdot \sum_{l \in \mathcal{I}_c^{(n)}} P_l^{(n)} \tau_l^{(n)} \\ \mathrm{angle}(\sum_{l \in \mathcal{I}_c^{(n)}} P_l^{(n)} \exp(j \cdot \varphi_{\mathrm{Rx},l}^{(n)})) \\ \mathrm{angle}(\sum_{l \in \mathcal{I}_c^{(n)}} P_l^{(n)} \exp(j \cdot \varphi_{\mathrm{Tx},l}^{(n)})) \end{bmatrix}, \end{aligned} \tag{1}$$

   where the mean angle is calculated by averaging angles over their respective complex representation.

   For tracking, also the centroid speed is of interest, so we combine the position and speed in the cluster tracking parameter vector $\boldsymbol{\theta}_c^{(n)} = [\tau_c^{(n)} \ \Delta\tau_c^{(n)} \ \varphi_{\mathrm{Rx},c}^{(n)} \ \Delta\varphi_{\mathrm{Rx},c}^{(n)} \ \varphi_{\mathrm{Tx},c}^{(n)} \ \Delta\varphi_{\mathrm{Tx},c}^{(n)}]^{\mathrm{T}}$.

5. The *cluster's joint spread* $\mathbf{C}_c^{(n)}$, which is the power-weighted covariance matrix of the path parameters within one cluster at time n. The main diagonal contains the cluster spreads of the individual dimensions, i.e. the cluster delay spread, the cluster AoA spread and the cluster AoD spread. The off-diagonal elements describe the correlation between these spreads.

   The cluster spread matrix is calculated by

$$\mathbf{C}_c^{(n)} = \frac{\sum_{l \in \mathcal{I}_c^{(n)}} P_l^{(n)} (\mathbf{x}_l^{(n)} - \boldsymbol{\mu}_c^{(n)})(\mathbf{x}_l^{(n)} - \boldsymbol{\mu}_c^{(n)})^{\mathrm{T}}}{\gamma_c^{(n)}}. \tag{2}$$

   Note that in this equation, whenever adding or subtracting angles, the result must be mapped to the principal value in the interval of $(-\pi, \pi]$, which can be achieved easily by the operation

$$\mathrm{pv}(\varphi) = \mathrm{angle}(\exp(j\varphi)). \tag{3}$$

Based on this cluster data model, we will now introduce the clustering-and-tracking framework.

3 Framework

For each time snapshot, the following steps are performed (see Figure 1):

1. A Kalman filter [17] both tracks the cluster position over time, and predicts the cluster position in the next snapshot.
2. The initial-guess routine provides a initial guess of the cluster centroids, taking the predicted cluster centroids into account.
3. The clustering algorithm identifies clusters in the measurement data based on the initial guess.

3.1 Kalman cluster tracking

3.1.1 State-space model

We consider linear cluster movement in delay and angles. For the Kalman tracking [17], only the cluster centroid position $\boldsymbol{\theta}_c$ is used. We use the following state equation

$$\boldsymbol{\theta}_c^{(n)} = \Phi\boldsymbol{\theta}_c^{(n-1)} + \mathbf{w}^{(n)}, \tag{4}$$

where $\mathbf{w}^{(n)}$ denotes the state-noise with covariance matrix $\mathbf{Q}$, and Φ is the state-transition matrix given by

$$\Phi = \mathbf{I}_3 \otimes \begin{bmatrix} 1 & 1 \\ 0 & 1 \end{bmatrix},$$

where identity matrices are denoted by $\mathbf{I}_d$ with d denoting the dimension, and $\otimes$ denotes the Kronecker matrix product.

Since we can observe only the cluster centroids and not their speed, we use the following observation model

$$\boldsymbol{\mu}_c^{(n)} = \mathbf{H}\boldsymbol{\theta}_c^{(n)} + \mathbf{v}^{(n)}, \tag{5}$$

where $\boldsymbol{\mu}_c^{(n)}$ describes the *observed* cluster centroid position, thus $\mathbf{H}$ is given by

$$\mathbf{H} = \mathbf{I}_3 \otimes [\ 1 \quad 0\ ], \tag{6}$$

and $\mathbf{v}^{(n)}$ denotes the observation noise with covariance matrix $\mathbf{R}$.

3.1.2 Tracking equations

The derivation of the Kalman filter is straight-forward and leads to following prediction and update equations[1]

Prediction:

$$\boldsymbol{\theta}_c^{(n|n-1)} = \Phi\boldsymbol{\theta}_c^{(n-1|n-1)}, \tag{7}$$

$$\mathbf{M}^{(n|n-1)} = \Phi\mathbf{M}^{(n-1|n-1)}\Phi^{\mathrm{T}} + \mathbf{Q}, \tag{8}$$

Update:

$$K^{(n|n)} = \mathbf{M}^{(n|n-1)}\mathbf{H}^{\mathrm{T}}(\mathbf{H}\mathbf{M}^{(n|n-1)}\mathbf{H}^{\mathrm{T}} + \mathbf{R})^{-1}, \tag{9}$$

$$\boldsymbol{\theta}_c^{(n|n)} = \boldsymbol{\theta}_c^{(n|n-1)} + K^{(n|n)}(\boldsymbol{\mu}_c - \mathbf{H}\boldsymbol{\theta}_c^{(n|n-1)}), \tag{10}$$

$$\mathbf{M}^{(n|n)} = (\mathbf{I} - K^{(n|n)}\mathbf{H})\mathbf{M}^{(n|n-1)}. \tag{11}$$

The identity matrix is used as initial value for $\mathbf{Q}$, $\mathbf{M}$ and $\mathbf{R}$.

[1] Note that the principal-value calculation rules apply for the angular dimensions

3.1.3 Cluster association

A major problem in multi-target tracking is how to associate the predicted with the identified cluster centroids. Usually, such an association is based on the Euclidean distance in parameter space. Since we are tracking clusters that show a certain extent in parameter space, the Euclidean distance does not provide a good association. Instead, we use the following probability-based method:

- The distance between a cluster with parameters ($\boldsymbol{\mu}_c,\ \mathbf{C}_c$) and a cluster centroid $\tilde{\boldsymbol{\mu}}$ is defined by

$$\mathcal{G}_c(\tilde{\boldsymbol{\mu}}|\boldsymbol{\mu}_c, \mathbf{C}_c) = \frac{1}{(2\pi)^{3/2}\,|\mathbf{C}_c|^{1/2}} \cdot \exp\left(-\frac{1}{2}(\tilde{\boldsymbol{\mu}} - \boldsymbol{\mu}_c)^{\mathrm{T}}\mathbf{C}_c^{-1}(\tilde{\boldsymbol{\mu}} - \boldsymbol{\mu}_c)\right). \tag{12}$$

  Since a small distance between the two centroids now corresponds to a large value of this function, we refer to it as the *closeness function*.

- The closeness function is evaluated between all predicted and all new cluster centroids in both directions, i.e. between the old and the new centroids using the old covariance matrix, and between the new and old cluster centroids using the new covariance matrix.

- For each old cluster we determine the closest new cluster by finding the maximum value of the closeness function, and vice versa, for each new cluster we determine the closest old cluster in the same way.

- Whenever these two clusters are closest mutually, these two clusters are associated and being considered as the *tracked* cluster.

- Clusters that were not associated from the old snapshot stop to exist, clusters that were not associated from the new snapshot are considered as new clusters.

3.2 Cluster initial guess

A crucial point in any iterative clustering algorithm is the initial guess of the cluster centroids. Our new method chooses the centroids by maximizing the distances between them. In the following we will present how to choose the initial-guess centroids $\hat{\boldsymbol{\mu}}_c$.

1. Initialization:
   - No cluster prediction available:
     The first centroid $\hat{\boldsymbol{\mu}}_1$ is chosen as the path having strongest power. Go to Step 2.
   - Cluster Prediction available:
     Copy the initial-guess centroids from the predicted values. Go to Step 4.

2. Calculate a weighted distance between any path and all (initial-guess) centroids using the multipath component distance (MCD) [19] by

$$D(\mathbf{x}_l^{(n)}, \hat{\boldsymbol{\mu}}_c) = \log_{10}(P_l^{(n)}) \cdot \mathrm{MCD}(\mathbf{x}_l^{(n)}, \hat{\boldsymbol{\mu}}_c).$$

   This leads to an $L \times c$ distance matrix $\mathbf{D}$ for every snapshot n. Here, the MCD is log-power weighted.

3. The new centroid is chosen from these paths, by selecting the one to which has the maximum minimum distance to any centroid, i.e. $l = \arg\max[\min_c \mathbf{D}]$, where $\arg\max[\cdot]$ returns the index of the maximum element.

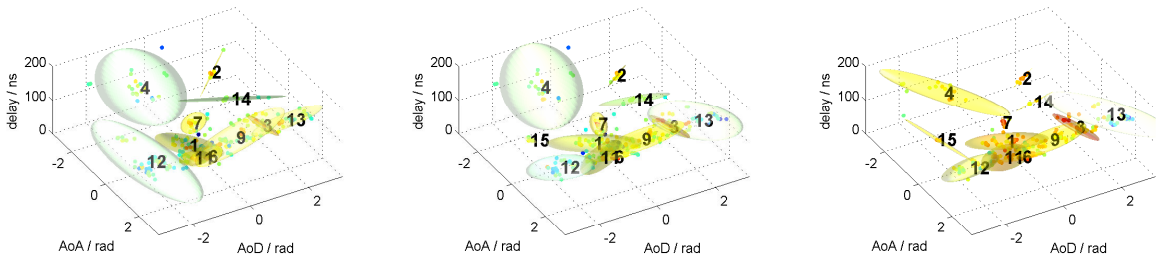

(a) (b) (c)

Figure 2: Tracked clusters from indoor scenario; (a)-(c) show the clusters' evolution over time

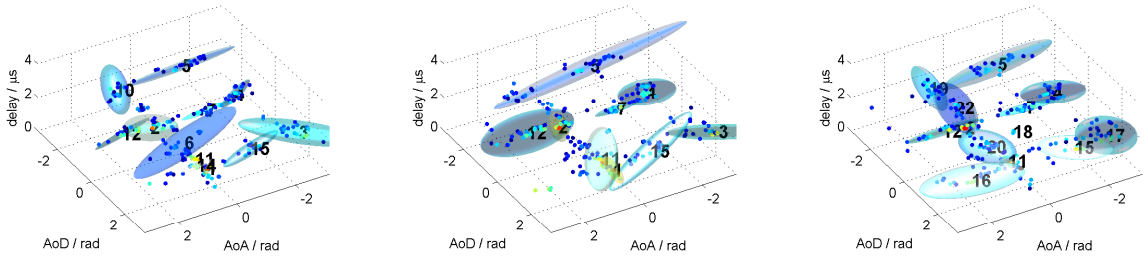

(a) (b) (c)

Figure 3: Tracked clusters from rural outdoor scenario; (a)-(c) show the clusters' evolution over time

4. Reallocate all paths to their closest centroid (as in the KPowerMeans algorithm) and calculate the cluster power. Note that, in this case, the power-weighted MCD is also used but the powers contribute linearly.

5. If the maximum number of clusters was not reached, and all centroid powers are larger then 1% of the total snapshot power, then repeat from Step 2.
   Else discard the last centroid and stop. This algorithm leads to a trustworthy identification of the number of clusters.

3.3 Clustering algorithm

We use the KPowerMeans clustering algorithm presented in [13] with following modifications: (i) we apply the initial guess as described above, (ii) since the initial guess is deterministic, the algorithm is performed only once.

Should the outcome result in clusters carrying less than 1% of the snapshot power, the result is discarded and the procedure is restarted with the initial guess, but reducing the maximum number of clusters by one. Note that in this algorithm the existence of singleton clusters is possible, as long as they show enough power. In this way we can also account for strong specular reflections.

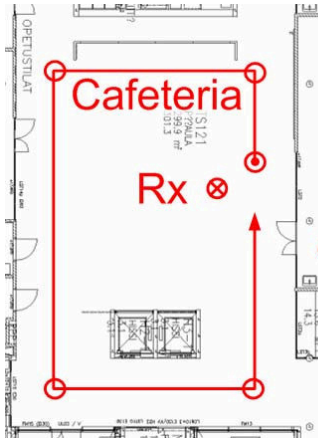

Figure 4: Floorplan of the indoor scenario

4 Measurements

In this paper we compare data from three different channel sounding campaigns conducted by different institutions.

4.1 Campaign I — indoor scenario

These measurements were conducted at the University of Oulu, Finland using an Elektrobit Propsound CS^{TM} wideband radio channel sounder at a center frequency of 2.55 GHz [14]. Snapshots of the radio channel were recorded approximately every 0.45λ. The recorded impulse responses were post-processed using the ISIS (initialization-and-search improved SAGE) algorithm to estimate single propagation paths [20].

In this paper we discuss results from a line-of-sight (LOS) measurement route in a cafeteria (see Figure 4). The Rx was placed on a table, while the Tx was moved along the indicated route in the room over a distance of 44 m corresponding to 295λ. Because of many metal chairs and tables, and the quite reflective walls, we expected rich scattering in the channel apart from the LOS component. However, it turned out that the observed channels were still pretty directive.

4.2 Campaign II — outdoor sub-urban environment

The data were collected in a small town called Weikendorf, northwest of Vienna, Austria. For the measurements we used a RUSK MEDAV channel sounder operating at a center frequency of 2.0 GHz [15]. Snapshots of the radio channel were recorded approximately every 1.6λ. The recorded impulse responses were also post-processed using the ISIS algorithm to estimate the propagation paths.

The measurement route (see Figure 5) was along a road towards a railway tunnel, mostly with LOS, partly with obstructed LOS. The total distance traveled was 53 m corresponding to 353λ. The channel is quite directive at the Rx side, but shows rich scattering around the Tx.

4.3 Campaign III — outdoor rural environment

The third set of measurements were conducted in an outdoor scenario in the 300 MHz band using the RUSK Lund MIMO channel sounder. A description of the measurement campaign can be found

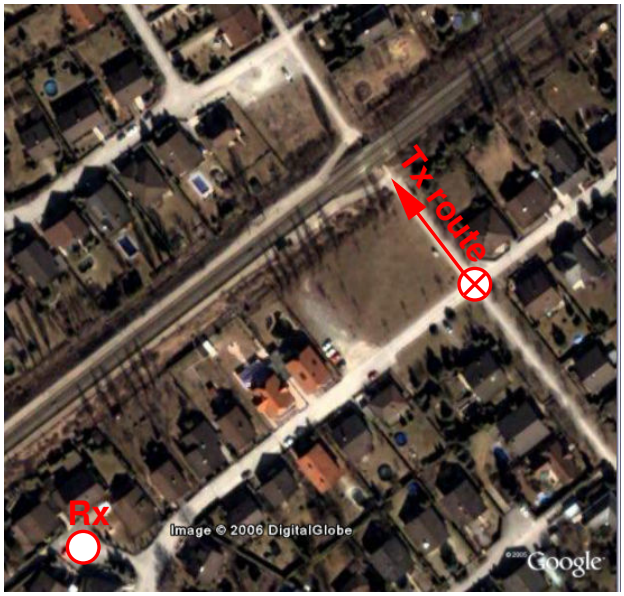

Figure 5: Sub-urban environment

in [21].

The measurement route used in this paper (see Figure 6) is approximately 320 m long, corresponding to 320λ. The snapshot spacing used in this paper is approximately 0.97λ. The measured impulse responses were post-processed by a SAGE algorithm [20] to obtain propagation paths for each snapshot of the channel.

5 Results

We applied our joint clustering-and-tracking framework to the three sets of measurements and found that the algorithm provides clusters that match well the time-varying physical propagation mechanisms observed in the measured scenarios. Exemplary plots from the indoor and the rural outdoor scenario are shown in Figures 2 and 3. The individual plots show the evolution over time. Propagation paths are marked by dots, their power is color coded from red (strong power) to blue (weak power). Clusters are shown by ellipsoids (capturing 99.9% of the power of the included paths), where the colour describes the mean power of the included paths, and the numbers indicate the cluster IDs placed at the cluster centroid.

This paper focuses on the *time-variance* of the cluster parameters, i.e. how much do the cluster parameters change during the existence of the individual clusters.

We focus on (i) the change of the cluster position over the traveled wavelength ("cluster movement"), (ii) the change of the cluster spreads, (iii) the cluster lifetime and cluster birth and death rates.

5.1 Cluster movement

Figure 7 exemplifies the cluster mean delay for one individually selected cluster from each environment. The cluster mean delay varies significantly in the presented indoor environment (Figure 7a), it seems that the cluster jitters around a steady increase. Also in the sub-urban environment (see

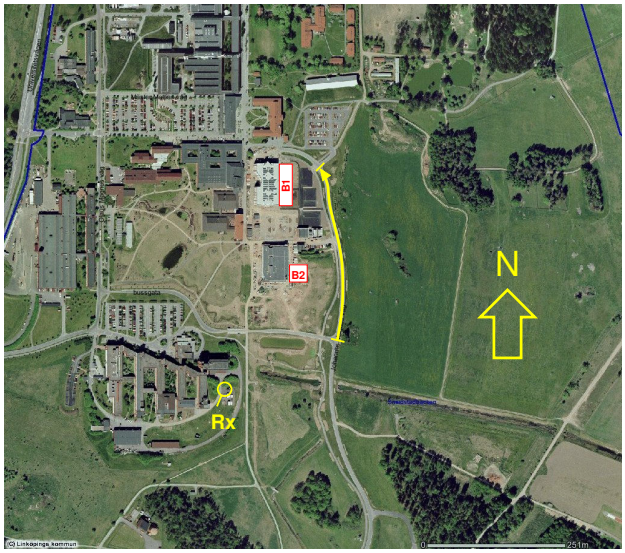

Figure 6: Rural environment

Figure 7b), the cluster is changing its position quite strongly over its lifetime. This cluster is likely to combine two scatterers. The steep decrease in delay is likely to come from a change in the propagation conditions, where the scatterer with shorter delay grew stronger, thus making the cluster delay smaller. In the rural environment (Figure 7c), the strong movement during the first few snapshots seems to be an artifact of the tracking algorithm. The Kalman tracking needs some training to keep track of the cluster. After these first snapshots, the cluster delay increases almost steadily.

We describe the cluster movement by the change of the cluster mean parameters related to traveling one wavelength with the transmitter. In the following we will present the average cluster movement of all clusters identified in the three environments. Since the sample mean of the parameters is strongly influenced by the artifacts, we decided to use the *median* of the sample instead. Figures 8–10 show histograms of these movement parameters. The mean cluster delay changes within the range of $-5 \ldots 5$ ns per wavelength (see Figure 8). Strong changes can again be attributed to the combination of more than one propagation effect in one cluster.

The median cluster changes in AoA (see Figure 9) are particularly interesting, since we observe significant differences in the histograms for the different environments. This effect can be attributed to the very different propagation environments. In the indoor scenario, there was strong scattering around both the Rx and Tx, leading also to stronger cluster movement around the Rx. In the sub-urban scenario, the observed values are quite small. The Rx did not experience local scattering since it was placed on a crane overlooking the environment. In the rural environment, there was also strong scattering around the Rx, where the movement of the Tx led to cluster movement on the Rx side. The mean cluster changes in AoD shown in Figure 10 are quite similar for all environments.

5.2 Change of cluster spreads

Another figure of merit is how much the cluster spreads change during the lifetime of a cluster. Figure 11 shows the cluster delay spread of one individually selected cluster for each of the environments. In all three environments we observe that the delay spread changes significantly over the traveled distance. These changes seem to be rather random. Moreover, we also observe some

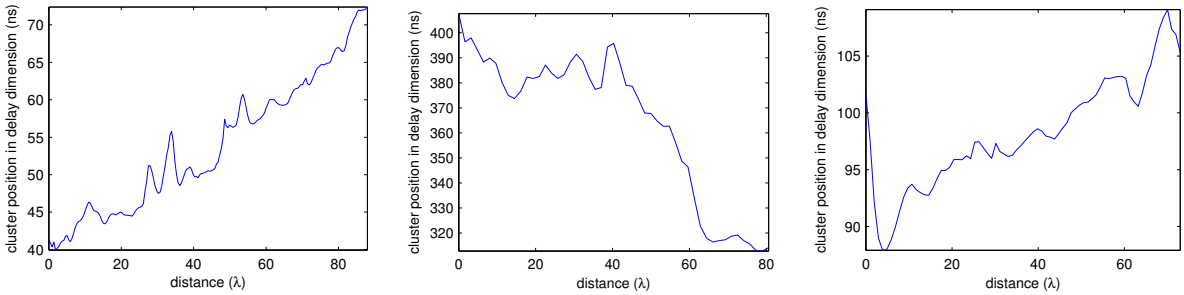

(a) indoor (b) sub-urban (c) rural

Figure 7: Cluster movement in delay dimension

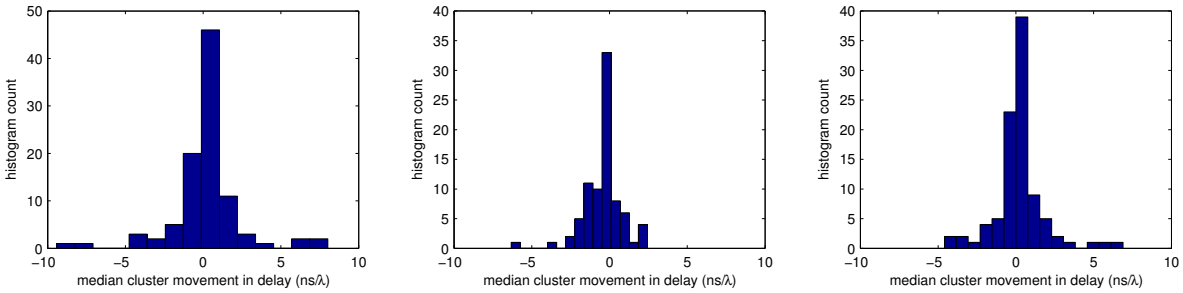

(a) indoor (b) sub-urban (c) rural

Figure 8: Median cluster movement in delay

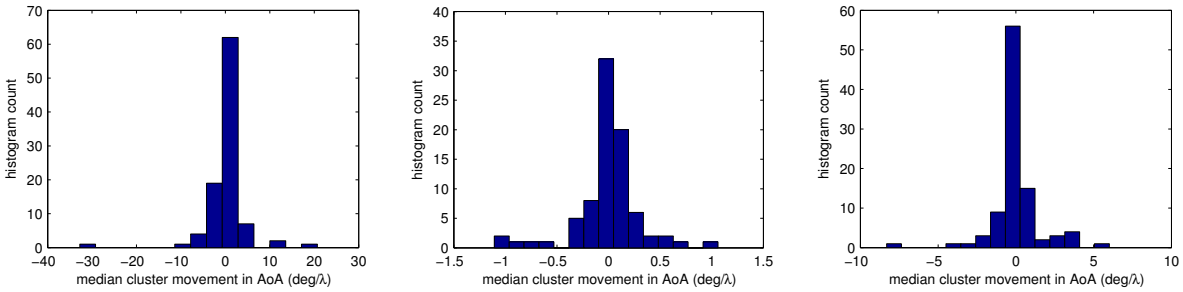

(a) indoor (b) sub-urban (c) rural

Figure 9: Median cluster movement in AoA

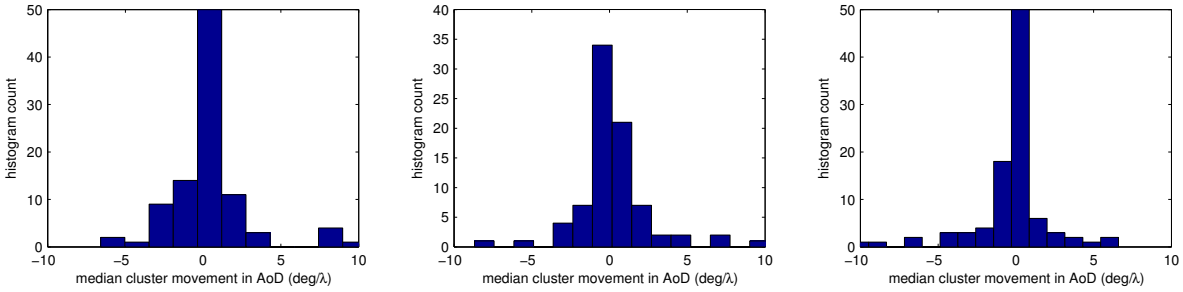

(a) indoor (b) sub-urban (c) rural

Figure 10: Median cluster movement in AoD

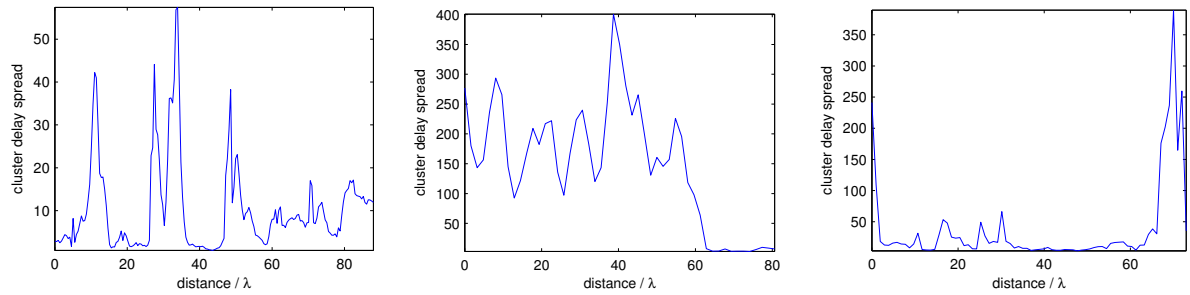

(a) indoor (b) sub-urban (c) rural

Figure 11: Change of the cluster delay spread

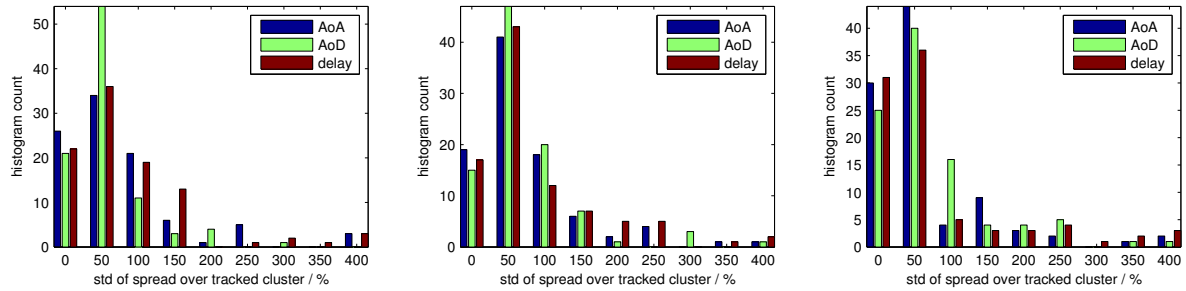

(a) indoor (b) sub-urban (c) rural

Figure 12: Standard deviations of the change of the cluster delay spreads in percent of the median delay spread

kind of outliers, which may again be an artifact of the clustering-and-tracking algorithm.

In order to quantify these changes, we use a deviation measure similar to the standard deviation of the cluster spread with following changes: (i) we use the median instead of the mean in order to mitigate the effect of outliers, (ii) we relate the deviation to the median value of the cluster spread to obtain a spread in percent. We calculate this spread deviation as

$$\mathcal{D}_\tau = \frac{\sqrt{\frac{1}{N}\sum_{k=1}^{N}(\sigma_{\tau,k} - \bar{\sigma}_\tau)^2}}{\bar{\sigma}_\tau},$$

where $\sigma_{\tau,k}$ denotes the cluster delay spread at snapshot k, $\bar{\sigma}_\tau$ denotes the cluster *median* delay spread over all snapshots, and N is the lifetime of the regarded cluster. The deviations for the AoA and AoD cluster spreads are defined similarly.

Figure 12 shows the the histograms of the deviation for all three cluster dimensions. We first observe a similar behavior for all three dimensions AoA, AoD and delay. a standard deviation around 50% of the cluster spread value is most probable. Surprisingly, the results are quite similar in all different environments. Values above 100% indicate that some clusters tend to grow for short periods, where they show considerably larger spreads than the median spread. In these cases, the clustering algorithm (accidentially, or for a good reason) combines wider-spread paths into one cluster. This effect occurs when some weak outlying propagation paths exist for just a few snapshots and then vanish again. Such paths are allocated to the closest cluster.

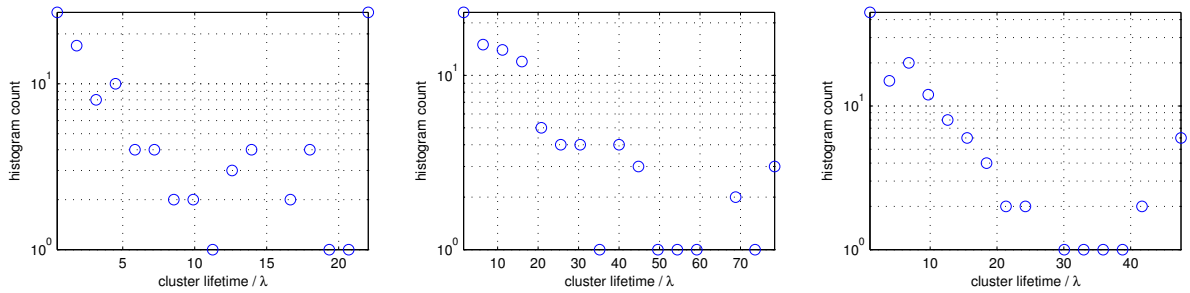

(a) indoor (b) sub-urban (c) rural

Figure 13: Cluster lifetimes in terms of wavelengths

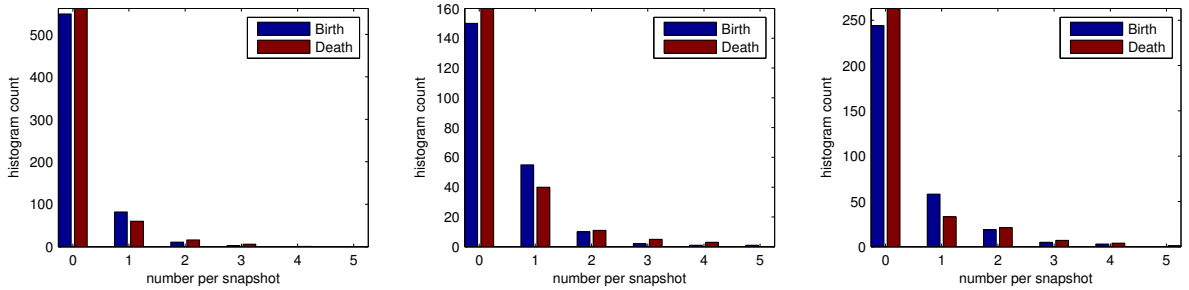

(a) indoor (b) sub-urban (c) rural

Figure 14: Cluster birth and death rate per snapshot

5.3 Cluster lifetimes, birth and death rates

Important parameters for cluster-based models are the lifetime of clusters and how strongly the number of clusters changes between different snapshots.

Figure 13 shows histograms of the cluster lifetimes for the different environments. Like in [15], the plots give rise to the assumption of an exponential distribution of the lifetime. However, we also observe a number of clusters with significantly larger lifetime. We particularly evaluated this effect for the rural environment and found that these long-living clusters come from the LOS path and from dominant reflectors in the channel. Thus, these clusters do have significant impact and must not be neglected when modeling the radio channel.

The birth rates and death rates of the clusters are evaluated in Figure 14. The histograms show the number of newly born or died clusters evaluated for all snapshots. It is evident that a change of one or two clusters in a snapshot is quite probable. Only in very few cases, three or more clusters are born or die at the same snapshot. Again, the results are fairly similar for all environments which leads to the conclusion that clusters can be tracked quite well.

6 Conclusions

This paper presented (i) a novel joint clustering-and-tracking algorithm in order to identify time-variant cluster parameters for geometry-based stochastic MIMO channel models, and (ii) we evaluated the time-variant behavior of multipath clusters from MIMO channel measurements in three different environments.

Using a Kalman filter to track the clusters and to predict the cluster position for the next time

instant significantly improves the ability to track clusters.

For tracking multiple clusters, we introduced a novel method for cluster association of predicted and identified clusters. By using the cluster spreads we could improve the cluster association considerably.

Applying the framework on three highly different types of MIMO channel measurements led to consistent results. The combination of tracking and clustering allows to identify the time-variant properties of clusters coherently.

The resulting cluster parameters show that clusters move significantly in the parameter domain. Some of these movements are quite strong, which can be attributed to changing propagation conditions in these particular clusters.

The cluster spreads are also strongly varying over the lifetime of the individual clusters with a deviation of up to 150 % around their median value. This effect is due to the allocation of short-living outlying paths to dominant clusters.

Cluster lifetimes are approximately exponentially distributed. However, the line-of-sight cluster, and clusters from dominant reflections need to be accounted for individually, since they show a much longer lifetime.

Our results show that the environment plays a significant role for the cluster movement parameters and for the cluster lifetimes, while the mean deviation of the spreads is quite similar in all environments.

Acknowledgements

This work was initiated by a short-term scientific mission in the framework of the EC project COST 2100. We thank Elektrobit Corp. for generous support. Research reported here was also supported by the Kplus program, an INGVAR grant from the Swedish SSF, and the SSF Center of Excellence for High-Speed Wireless Communications. We acknowledge the Swedish Defence Research Agency (FOI) for providing the 300 MHz measurement data.

References

[1] P. Almers, E. Bonek, A. Burr, N. Czink, M. Debbah, V. Degli-Esposti, H. Hofstetter, P. Kyösti, D.Laurenson, G. Matz, A. Molisch, C. Oestges, and H. Özcelik, "Survey of channel and radio propagation models for wireless MIMO systems," *EURASIP Journal on Wireless Communications and Networking*, 2007.

[2] "Spatial channel model for Multiple Input Multiple Output (MIMO) simulations (3GPP TR 25.996), v6.1.0," Sep. 2003. [Online]. Available: www.3gpp.org

[3] V. Erceg *et al.*, "TGn Channel Models," IEEE P802.11 Wireless LANs, Tech. Rep., May 2004, http://www.802wirelessworld.com:8802/.

[4] L. Correia, Ed., *Mobile Broadband Multimedia Networks*. Academic Press, 2006.

[5] Q. H. Spencer, B. D. Jeffs, M. A. Jensen, and A. L. Swindlehurst, "Modeling the statistical time and angle of arrival characteristics of an indoor multipath channel," *IEEE Journal on Selected Areas in Communications*, vol. 18, pp. 347 – 359, March 2000.

[6] C.-C. Chong, C.-M. Tan, D. Laurenson, S. McLaughlin, M. Beach, and A. Nix, "A new statistical wideband spatio-temporal channel model for 5-GHz band WLAN systems," *IEEE Journal on Selected Areas in Communications*, vol. 21, no. 2, pp. 139 – 150, Feb. 2003.

[7] M. Toeltsch, J. Laurila, A. F. Molisch, K. Kalliola, P. Vainikainen, and E. Bonek, "Spatial characterization of urban mobile radio channels," *IEEE JSAC*, vol. 20, pp. 539–549, 2002.

[8] K. Li, M. Ingram, and A. Van Nguyen, "Impact of clustering in statistical indoor propagation models on link capacity," *IEEE Transactions on Communications*, vol. 50, no. 4, pp. 521 – 523, April 2002.

[9] A. F. Molisch, "Effect of far scatterer clusters in MIMO outdoor channel models," in *Proc. 57th IEEE Vehicular Techn. Conf.*, 2003, pp. 534–538.

[10] N. Czink, E. Bonek, L. Hentilä, J.-P. Nuutinen, and J. Ylitalo, "A measurement-based random-cluster MIMO channel model," in *IEEE Antennas and Propagation Symposium 2007*, Honolulu, USA, June 2007.

[11] K. Yu, Q. Li, D. Cheung, and C. Prettie, "On the tap and cluster angular spreads of indoor WLAN channels," in *Proceedings of IEEE Vehicular Technology Conference Spring 2004*, Milano, Italy, May 17–19, 2004.

[12] N. Czink, P. Cera, J. Salo, E. Bonek, J.-P. Nuutinen, and J. Ylitalo, "Automatic clustering of MIMO channel parameters using the multi-path component distance measure," in *WPMC'05*, Aalborg, Denmark, Sept. 2005.

[13] ——, "A framework for automatic clustering of parametric MIMO channel data including path powers," in *IEEE Vehicular Technology Conference 2006 Fall*, Montreal, Canada, 2006.

[14] N. Czink, E. Bonek, L. Hentilä, J.-P. Nuutinen, and J. Ylitalo, "Cluster-based MIMO channel model parameters extracted from indoor time-variant measurements," in *IEEE GlobeCom 2006*, San Francisco, USA, Nov. 2006.

[15] N. Czink, G. D. Galdo, and C. F. Mecklenbräuker, "A novel cluster tracking algorithm," in *IEEE Personal Indoor and Mobile Radio Communications (PIMRC) 2006*, September 2006.

[16] J. Salmi, A. Richter, and V. Koivunen, "Enhanced tracking of radio propagation path parameters using state-space modeling," in *14th European Signal Processing Conference (EUSIPCO)*, Florence, Italy, September 2006.

[17] S. M. Kay, *Fundamentals of Statistical Signal Processing, Estimation Theory.* Prentice Hall, 1993.

[18] S. Wyne, N. Czink, J. Karedal, P. Almers, F. Tufvesson, and A. F. Molisch, "A cluster-based analysis of outdoor-to-indoor office MIMO measurements at 5.2 GHz," in *IEEE VTC Fall*, Montreal, Canada, 2006.

[19] N. Czink, P. Cera, J. Salo, E. Bonek, J.-P. Nuutinen, and J. Ylitalo, "Improving clustering performance by using the multi-path component distance," *IEE Electronics Letters*, vol. 42, no. 1, pp. 44–45, Jan. 2006.

[20] B. Fleury, P. Jourdan, and A. Stucki, "High-resolution channel parameter estimation for MIMO applications using the SAGE algorithm," in *2002 International Zurich Seminar on Broadband Communications*, Zurich, Feb. 2002, pp. 30–1 – 30–9.

[21] G. Eriksson, F. Tufvesson, and A. F. Molisch, "Propagation channel characteristics for peer-to-peer multiple antenna systems at 300 MHz," in *IEEE GlobeCom 2006*, San Francisco, USA, Nov. 2006.